nature materials

ARTICLES

PUBLISHED ONLINE: 25 OCTOBER 2009 | DOI: 10.1038/NMAT2545

Porous organic cages

Tomokazu Tozawa[1,2], James T. A. Jones[1], Shashikala I. Swamy[1], Shan Jiang[1], Dave J. Adams[1], Stephen Shakespeare[1], Rob Clowes[1], Darren Bradshaw[1], Tom Hasell[1], Samantha Y. Chong[1], Chiu Tang[3], Stephen Thompson[3], Julia Parker[3], Abbie Trewin[1], John Bacsa[1], Alexandra M. Z. Slawin[4], Alexander Steiner[1] and Andrew I. Cooper[1]*

Porous materials are important in a wide range of applications including molecular separations and catalysis. We demonstrate that covalently bonded organic cages can assemble into crystalline microporous materials. The porosity is prefabricated and intrinsic to the molecular cage structure, as opposed to being formed by non-covalent self-assembly of non-porous sub-units. The three-dimensional connectivity between the cage windows is controlled by varying the chemical functionality such that either non-porous or permanently porous assemblies can be produced. Surface areas and gas uptakes for the latter exceed comparable molecular solids. One of the cages can be converted by recrystallization to produce either porous or non-porous polymorphs with apparent Brunauer–Emmett–Teller surface areas of 550 and 23 $m^2 g^{-1}$, respectively. These results suggest design principles for responsive porous organic solids and for the modular construction of extended materials from prefabricated molecular pores.

Most molecules pack efficiently in the solid state to form structures with minimal void volume. As a result, covalent organic molecules with conventional permanent porosity are rare in comparison with extended porous networks, the latter of which have applications in catalysis, gas storage and molecular separations[1–4]. Organic clathrates, for example, tend to be unstable to guest removal and do not usually retain permanent pore structures[1]. Organic molecules that defy this rule include certain calixarenes[5–7], carbon nanotubes[8], *tris-o*-phenylenedioxycyclotriphosphazene[9] (TPP), 4-hydroxyophenyl-2,3-4-trimethylchroman[10], cucurbit[6]uril[11], and, recently, some dipeptides[12]. Metal–organic polyhedra can also show permanent porosity[13], which points to broader potential for porosity in 'molecularly panelled'[14] coordination assemblies.

Stable porous organic molecules might have advantages for some applications with respect to extended networks. For example, unlike networks, many molecules are solution processable. The advantage of this was illustrated recently with polymers of intrinsic microporosity[15], which can be cast from solution to form porous membranes. Moreover, soluble porous molecules promise rich derivatization chemistry, 'mix and match' assembly strategies and the possibility of purification by means of standard solution-phase procedures such as recrystallization and chromatography. The non-covalent nature of porous molecular assemblies also opens the way for highly guest-responsive materials[16].

The primary synthetic challenge is to prepare permanently porous organic crystals assembled using non-covalent forces, which are much weaker than the directional bonding in crystalline networks such as covalent organic frameworks[4,17,18]. We show that tetrahedral organic cages can be synthesized and subsequently desolvated to generate porous crystals that adsorb small gas molecules, such as nitrogen, hydrogen, methane and carbon dioxide. The crystal porosity in these materials is a consequence of both the molecular voids in the cages and the inefficient packing of tetrahedra[19,20]. We show that pore structure and connectivity is strongly directed by steric groups attached to the cage vertices such that it is possible to connect or disconnect the molecular void volumes in the covalent cages. This provides a new design principle for preparing highly porous organic materials by the synthetically directed assembly of prefabricated molecular pores. We anticipate that our findings will stimulate the development of totally new materials, such as porous liquids and structures showing 'on/off' porosity through the interconversion of polymorphs. These concepts arise from the discrete molecular nature of the cages, which contain fixed prefabricated covalent voids that are not generated by dynamic self-assembly processes, unlike for example calixarenes[5]. In contrast to coordination polyhedra[13,14,21], these cage materials are wholly organic and composed entirely of covalent C–C, C–H, N–H and C–N bonds.

Three imine-linked[22,23] tetrahedral cages were synthesized by the condensation reaction of 1,3,5-triformylbenzene with 1,2-ethylenediamine (cage **1**, 792 g mol^{-1}), 1,2-propylenediamine (cage **2**, 876 g mol^{-1}) and (*R*,*R*)-1,2-diaminocyclohexane (cage **3**, 1,118 g mol^{-1}; ref. 24) in a [4 + 6] cycloimination (see Supplementary Information for detailed experimental methods). The syntheses are carried out at room temperature and require no extra template, other than solvent. Products were isolated directly as crystalline solids, which were characterized by single-crystal X-ray diffraction. For example, **1** crystallized from ethyl acetate in monoclinic space group $C2/c$ as the solvate **1**:2.5 ethyl acetate, incorporating one cage molecule per asymmetric unit. The van der Waals packing coefficients for the cage-bound and interstitial ethyl acetate solvent molecules in solvated **1** were calculated to be 57.7% and 57.3%, respectively; that is, the solvent guest fills around 57% of the potential free volume in the material as calculated from the atomic van der Waals radii. This follows the '55% solution', where it was hypothesized by others[25] that 55% filling represents the best compromise between entropic freedom for the encapsulated

[1]Department of Chemistry and Centre for Materials Discovery, University of Liverpool, Crown Street, Liverpool L69 7ZD, UK, [2]Corporate Research & Development Division, Kaneka Corporation 5-1-1, Torikai-Nishi, Settsu, Osaka 566-0072, Japan, [3]I11 Beamline, Diamond Light Source Limited, Harwell Science and Innovation Campus, Chilton, Didcot OX11 0DE, UK, [4]School of Chemistry, University of St Andrews, North Haugh, St Andrews KY16 9ST, UK. *e-mail: aicooper@liv.ac.uk.

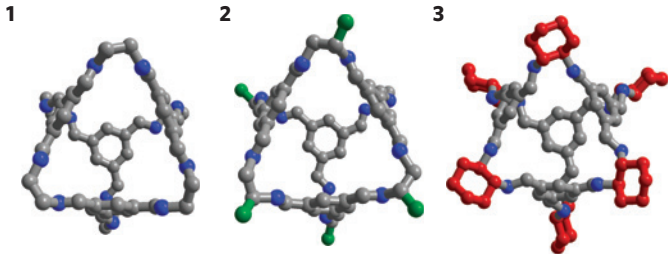

Figure 1 | Structures for cages 1–3 determined by X-ray crystallography for desolvated cages, as shown with one of the triangular pore windows facing. Hydrogen atoms are omitted for clarity. Carbon and nitrogen atoms are coloured grey and blue, respectively. The methyl and cyclohexyl groups on the vertices of cages **2** and **3** are shown in green and red, respectively. A single isomer is given for cage **2** (the 3111 isomer, see Fig. S20); the actual sample contains four separate positional isomers in which all methyl groups occupy exo sites.

guest and the enthalpic gain achieved by close contact between the host and the guest.

Cage **2** crystallized from acetonitrile in trigonal space group $P\bar{3}$, whereas cage **3** crystallized from dichloromethane or chloroform as a solvate with cubic $F4_132$ symmetry. The materials were fully desolvated to produce crystalline products **1–3** either by slow temperature ramping in a thermogravimetric analyser or by simple heating in air. In the case of **2**, the acetonitrile solvent was lost spontaneously under ambient conditions within around 30 min (Supplementary Figs S14–S19). Whereas **3** retained the original crystal structure and symmetry after thermal desolvation, crystals of **1** underwent a crystal-to-crystal transformation to monoclinic $P2_1/c$ symmetry after solvent removal by slow heating with a concomitant unit-cell volume decrease of 12%. The structures for **1–3**, as determined by X-ray diffraction, are shown in Fig. 1. Powder X-ray diffraction data correlated with simulations from single-crystal diffraction (Supplementary Figs S22–S24), thus demonstrating that the bulk materials were structurally representative of the single crystals chosen for analysis.

The core cage structure for **1–3** shows tetrahedral symmetry (point group T; refs 26–28). Four $C_6(CN)_3$ units of planar three-fold symmetry are linked by six aliphatic 1,2-diamine moieties. The resulting cages **1**, **2** and **3** each feature four approximately triangular windows with effective diameters of 5.8, 6.1 and 5.8 Å, respectively, as calculated from radii measured from the centre of the window to the three arene hydrogens (less half of the van der Waals radius for hydrogen, see Supplementary Fig. S21). The rigid cage structure locks the six vertex groups in a staggered conformation with fixed exo/endo sites. As a result, the cages are chiral and the six vertices are optically equivalent. Molecules **1–3** vary in the steric groups that are attached to the exo sites of the vertex linkers. Cage **1** has unfunctionalized ethylene vertices, whereas **2** has one exo-methyl group per vertex (shown in green). The vertices of **3** consist of relatively bulky cyclohexyl groups (red). It should be noted that cage **2** can exist as four separate isomers bearing distinct arrangements of exo-methyl groups, as indicated by positional disorder of methyl groups over the exo sites (Supplementary Fig. S20).

The crystallographic packing and hence the pore structure in these materials is dictated by the tetrahedral cage symmetry and by the exo-structure-directing groups on the cage vertices (Fig. 2). As crystallized from ethyl acetate, cage **1** packs in window-to-arene stacks (Fig. 2a) and these stacks are arranged window-to-ethylene with respect to each other to give a relatively dense structure with a calculated crystal density 1.033 g cm^{-3} and with no inter-cage window connectivity. Cage **1** is therefore formally non-porous but has isolated lattice voids, represented by the orange Connolly surface representation in Fig. 3a, which

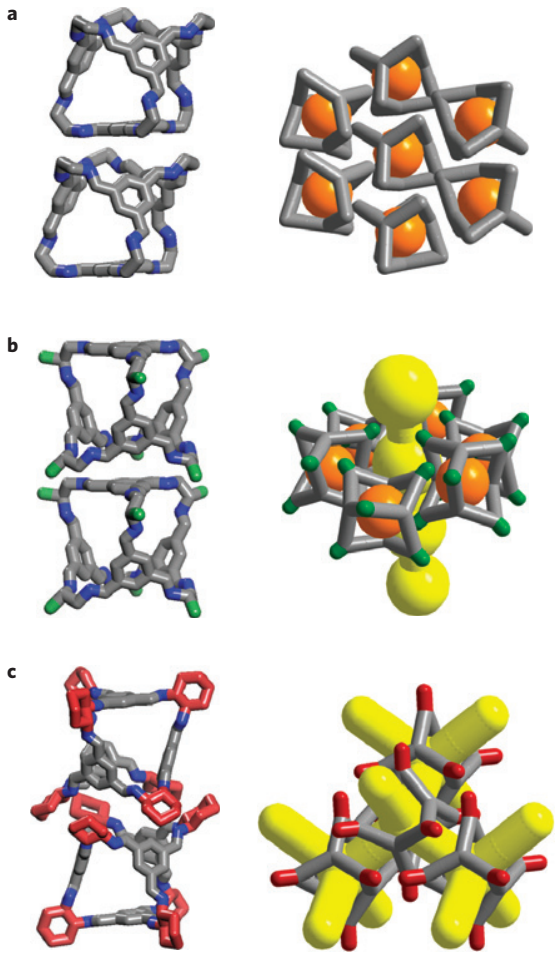

Figure 2 | Schematic of cage–cage packing in the crystal structures of 1–3. a, Two adjacent molecules of **1** pack in a window-to-arene fashion. These window-to-arene 'stacks' are arranged in a pseudo-hexagonal manner resulting in isolated void volume, as illustrated here in orange. **b**, Cage **2** forms similar window-to-arene stacks, which also generates isolated void volume (orange), but the methyl groups (shown in green) frustrate packing to give inter-stack 1D pore channels (yellow), which are encircled by the cage voids. **c**, Cage **3** is directed by the cyclohexyl groups (red) to pack window-to-window, thus generating an interconnected diamondoid-pore network, as illustrated here in yellow.

are reminiscent of calixarenes[5] and resorcinarenes[29] but generated here inside a single covalent organic molecule rather than within a self-assembled dimer or multicomponent capsule[30]. Cage **2** packs in an analogous manner (Fig. 2b), but packing of the resulting stacks is frustrated by the six vertex methyl groups, as reflected by the reduced crystallographic density (0.874 g cm^{-3}). This leads to a one-dimensional (1D) undulating pore channel running between the cages as coloured yellow in Fig. 3b. The necks of these channels are defined by the methyl groups on neighbouring cages and have an approximate diameter of 6.2 Å, whereas the channel cavities have a diameter of 14.0 Å at the widest point. The windows in cage **2** face away from these channels and hence the cage voids represented by the orange Connolly surface in Fig. 3b do not connect with the channel volume. The 1D channels are similar to those observed in a microporous trigonal β-form polymorph of a copper-linked coordination framework[31,32].

Unlike **1** and **2**, cage **3** packs in a window-to-window arrangement (Fig. 2c). Interlocking of three cyclohexyl groups on adjacent cages causes the windows in **3** to align. Combined with the tetrahedral cage symmetry, this results in an interconnected

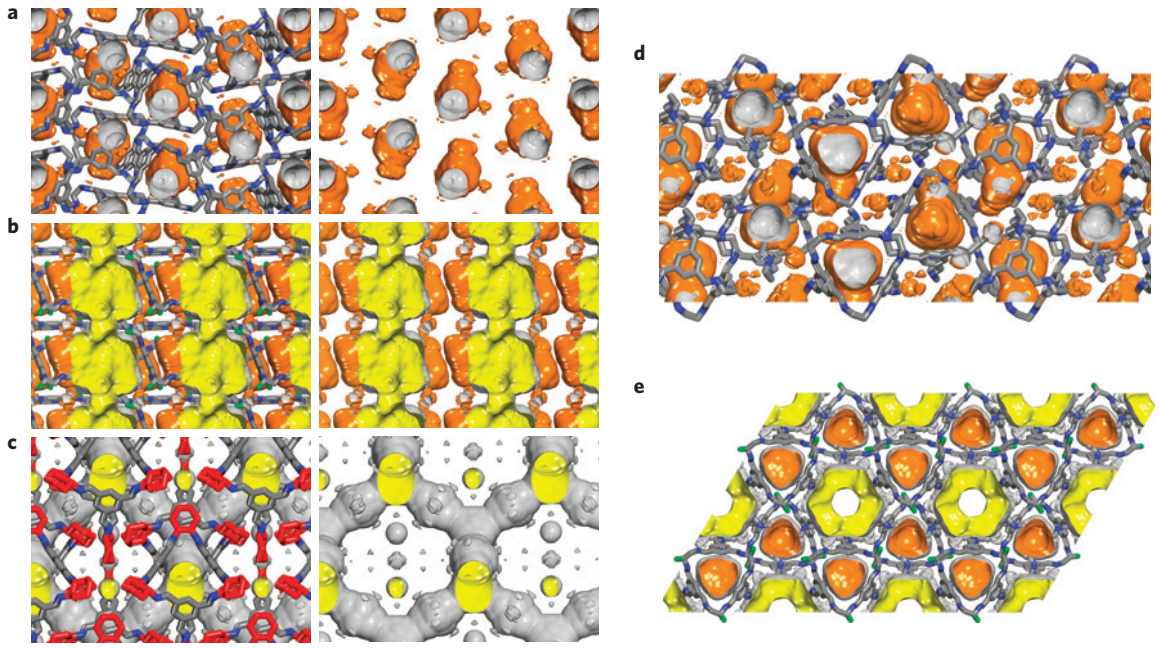

Figure 3 | Varying the vertex functionality for cages 1–3 leads to an evolution in pore structure and connectivity. a, Cage **1** has isolated lattice voids, as illustrated by the orange Connolly surface (probe radius = 1.82 Å) applied to the crystal structure for the desolvated material. The cross-sectional image on the right shows the structure without the cage framework, illustrating the lack of void connectivity. **b**, The positionally disordered methyl groups on the vertices of **2** (shown in green) direct the crystal packing to give an undulating 1D pore channel between the cages (the yellow Connolly surface in this cross-section through the centre of the channels). The cage void volume (orange surface) is not interconnected, nor does it connect with the 1D pore channel. The disordered methyl groups were positioned in this model according to the 2220 isomer for **2**, see also Supplementary Fig. S4. **c**, The more bulky cyclohexyl groups (red) in **3** direct the cages to pack window-to-window, leading to an interconnected diamondoid-pore channel structure (yellow). Unlike the 1D pores in **2**, this runs through the cages. **d**,**e**, Perpendicular cross-sections for crystal structures of **1** (**d**) and **2** (**e**). The 1D pore channel in **2** is surrounded by six stacks of disconnected cage voids.

3D diamondoid channel structure (Fig. 3c) running through rather than between the cages. The channel diameter in **3** varies between 5.8 Å at the narrowest point within the triangular cage window to 7.2 Å within the cage itself. The pore necks apparent in the crystal structures for cages **2** and **3** (6.2 and 5.8 Å, respectively) are close to the diameters measured by gas sorption for certain narrow-pore copper-based metal–organic frameworks (6.5 Å; ref. 33) and larger than observed in the channel structure of TPP (4.6 Å; ref. 9). Pore size distributions calculated by non-local density functional theory from N_2 sorption analyses for cages **2** and **3** are in broad agreement with the crystallographic measurements (Supplementary Fig. S28) and show well-defined peaks in the micropore region. Such direct comparisons must however be treated with caution because there is potential for these molecular materials to change structure in response to gas sorption, as observed at modest gas pressures (<1 atm) in covalently linked microporous polymer networks[34]. It should be noted that all X-ray structures were obtained for samples mounted under ambient conditions, rather than materials that are outgassed and held under high vacuum. Powder X-ray diffraction for **2** showed that no permanent structural change occurred after gas sorption and desorption (Supplementary Fig. S23), but this does not preclude a structural response during sorption starting from the fully outgassed, guest-free state.

All of the desolvated cage structures were found to adsorb significant quantities of gases but under different physical conditions. Cage **1** adsorbs little N_2 or H_2 compared with **2** and **3** at 77.3 K, but adsorbs relatively larger quantities of CH_4 and CO_2 close to ambient temperature (Fig. 4a–d), thus showing porosity 'without pores'[1]. This is consistent with the disconnected void structure in **1** (Fig. 3a) and implies a dynamic cooperative diffusion mechanism[35]. In contrast, **2** shows a type I N_2 sorption isotherm (Fig. 4a) and adsorbs a total of 7.52 mmol g^{-1} N_2 at 77.3 K and a relative pressure (P/P_0) of 0.998. The Langmuir surface area calculated for **2** from the N_2 isotherm was 600 m^2 g^{-1} and the Brunauer–Emmett–Teller surface area (SA_{BET}) was 533 m^2 g^{-1}. Cage **3** also shows a type I N_2 sorption isotherm with a corresponding Langmuir surface area of 730 m^2 g^{-1} (SA_{BET} = 624 m^2 g^{-1}).

Cage **1** adsorbs broadly similar absolute molar quantities of the four different gases studied (0.44–1.27 mmol g^{-1} up to one bar, Supplementary Table S1), but far less gas relative to **2** and **3** at cryogenic temperatures. The relative gas sorption capacities for **1**–**3** are therefore not solely a consequence of crystallographic density and unoccupied volume. The sorption trends are consistent with the crystallographic structures: **1** has no formally connected pores, whereas both **2** and **3** show interconnected permanent pore structures and adsorb significant volumes of gases at cryogenic temperatures and low pressures (<1 bar).

These cage materials have lower surface areas and accessible pore volumes than many extended networks[2–4,17,18], but the gas uptakes exceed reports for other discrete organic molecules. For example, **3** adsorbs 8.17 mmol g^{-1} N_2 in comparison with 2.6 mmol g^{-1} for TPP, 3.8 mmol g^{-1} for cucurbit[6]uril[11] and 4.0 mmol g^{-1} for 1,2-dimethoxy-*p*-*t*-butylcalix[4]dihydroquinone[6]. The metal–organic polyhedron, IRMOP-51, was reported to adsorb 6.1 mmol g^{-1} N_2 under comparable conditions[13]. Few hydrogen-sorption measurements have been published for permanently porous organic crystals, but **2**, for example, adsorbs 8.88 mmol g^{-1} H_2 (1.75 wt%) at 77.3 K and 7 bar (Supplementary Fig. S33). In comparison, a porous dipeptide, L-isoleucyl-L-valine, was recently shown to adsorb 2.3 mmol g^{-1} H_2 (0.45 wt%) under equivalent conditions[12]. Cages **2** and **3** also adsorb substantial quantities of CO_2 and CH_4 (Fig. 4c,d): **2** adsorbs 3.0 mmol g^{-1} (13.2 wt%) CO_2 at 275 K and 1.12 bar (Fig. 4d) and 5.48 mmol g^{-1} (24.1 wt%) at 290 K and 12 bar (Supplementary Fig. S34). Volumetric rather than gravimetric gas

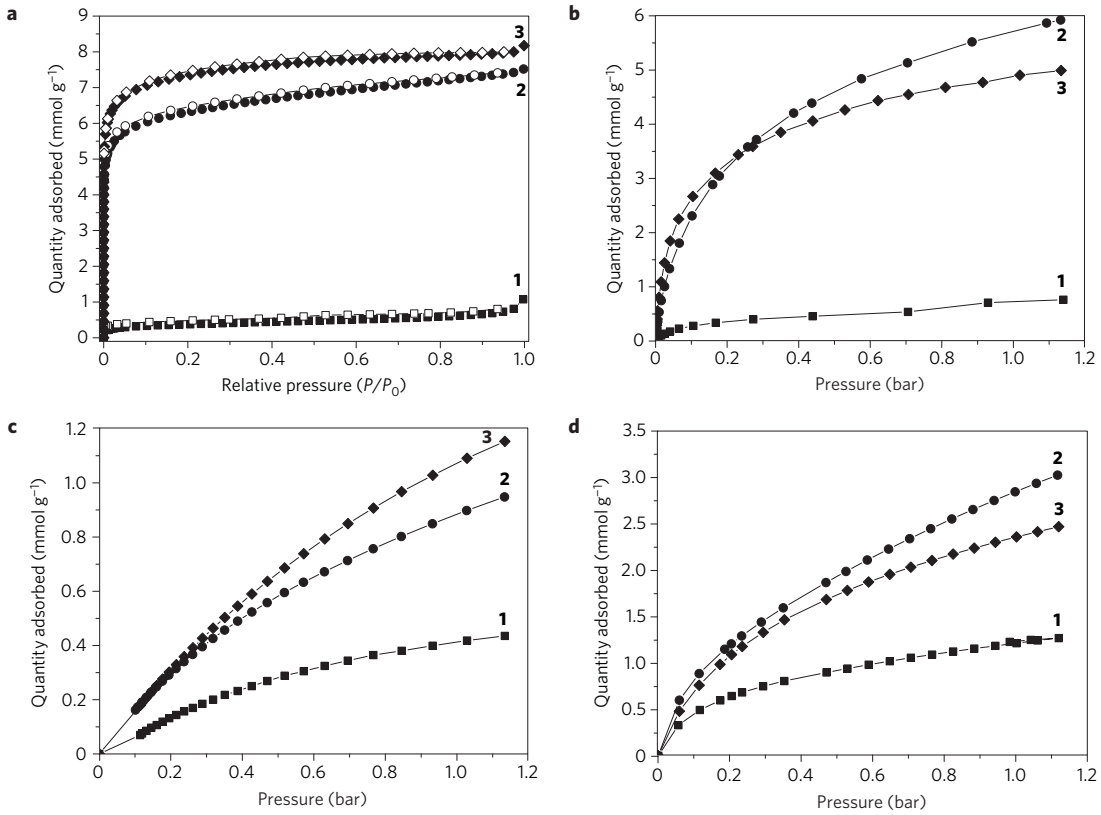

Figure 4 | Gas-sorption isotherms for cages 1–3. a, Reversible nitrogen-sorption isotherms for cages **1**–**3**. Filled and open symbols represent adsorption and desorption, respectively. The Langmuir surface areas derived from the adsorption isotherms are: (**1**) 40 $m^2\ g^{-1}$; (**2**) 600 $m^2\ g^{-1}$ ($SA_{BET} = 533\ m^2\ g^{-1}$), and; (**3**) 730 $m^2\ g^{-1}$ ($SA_{BET} = 624\ m^2\ g^{-1}$). **b**–**d**, Hydrogen (**b**), methane (**c**) and carbon dioxide (**d**) adsorption isotherms for cages **1**–**3**.

sorption capacities for these cages compare more favourably with porous networks because of the relatively high crystallographic density for cages **1**–**3** and the fact that these materials are composed exclusively of light elements, a general advantage of organic materials. For example, the volumetric CO_2 capacity for **2** is comparable to those reported for zeolitic imidazolate frameworks[36]. The CO_2 capacity and sorption selectivity might be improved further, for example, by chemical reduction of the imine cages to the corresponding amines.

The gas sorption observed in non-porous **1** prompted us to consider the possible contribution of the formally disconnected zero dimensional (0D) cages in **2**. X-ray diffraction experiments demonstrated the presence of disordered physisorbed guests in both the 1D channels and 0D cages of **2** (Fig. 5a). Complementary analytical methods (Fourier-transform infrared, ^{1}H NMR) showed that these guests were mostly physisorbed water. These X-ray data show that the 0D cage volume is available for guest sorption, at least in the case of water physisorption under ambient conditions. Molecular simulations (Fig. 5b) of N_2 sorption in **2** located three most favourable sorption sites: the 1D channel perimeter (site 1 in Fig. 5c,d), the narrow 1D channel neck (site 2) and the 0D cavities (site 3), with sites 1 and 3 showing the highest calculated relative binding energies. A maximum of 12.5 N_2 molecules per unit cell was calculated when both the 0D cavities and 1D channels were available for gas sorption, in good agreement with the measured N_2 uptake at saturation (Fig. 4a) of 12.7 N_2 molecules per unit cell. In contrast, a maximum of 7 N_2 molecules per unit cell was calculated by simulations that excluded the 0D cavities. In combination with the X-ray diffraction data shown in Fig. 5a, this strongly suggests that both the 1D channel and the 0D cavities accommodate N_2 at saturation. Cage **1** behaves differently, adsorbing little N_2 in its 0D cavities at 77 K (Fig. 4a). This difference may be partly kinetic in origin because **2**, unlike **1**, is permeated by 1D pore channels and each 0D cavity is surrounded by three near-neighbour channels at a cage-centre to channel-centre distance of 1.037 nm.

Cages **1**–**3** have relatively good thermal stability and the desolvated materials show an onset of decomposition at >600 K, as measured by thermogravimetric analysis (Supplementary Figs S16–S18). Samples were also reanalysed after gas-sorption measurements by solution-phase ^{1}H NMR and powder X-ray diffraction to ensure that there was no evidence of chemical decomposition or changes in the crystal structure as a result of the outgassing procedure, which involved heating to 353 K under dynamic vacuum. The stability of the desolvated crystals was further demonstrated by *in situ* single-crystal X-ray diffraction analysis for **3**, which showed that heating to 400 K in a dry N_2 stream caused no loss of crystallinity.

The molecular nature of these organic cages permits solution processing into a variety of forms. For example, we have found that **1**, which is formally non-porous as synthesized from ethyl acetate ($SA_{BET} = 24\ m^2\ g^{-1}$), can be recrystallized from a mixture of dichloromethane and *o*-xylene to form a permanently porous polymorph ($SA_{BET} = 550\ m^2\ g^{-1}$; Fig. 6). Le Bail fitting of powder X-ray diffraction data obtained after desolvation of this polymorph suggests a similar packing mode to that observed for cage **2** but with reduced symmetry (Supplementary Fig. S39). This further underlines the differences between these porous molecular cages and insoluble organic networks, such as covalent organic frameworks[4,17,18], which have extended structures that are defined by rigid, directional covalent bonds.

We have demonstrated that it is possible to synthetically direct the porosity in molecular organic materials from closed voids (**1**) to a combination of voids and 1D pore channels (**2**) through to 3D pore networks (**3**) by changing the cage vertex functionality.

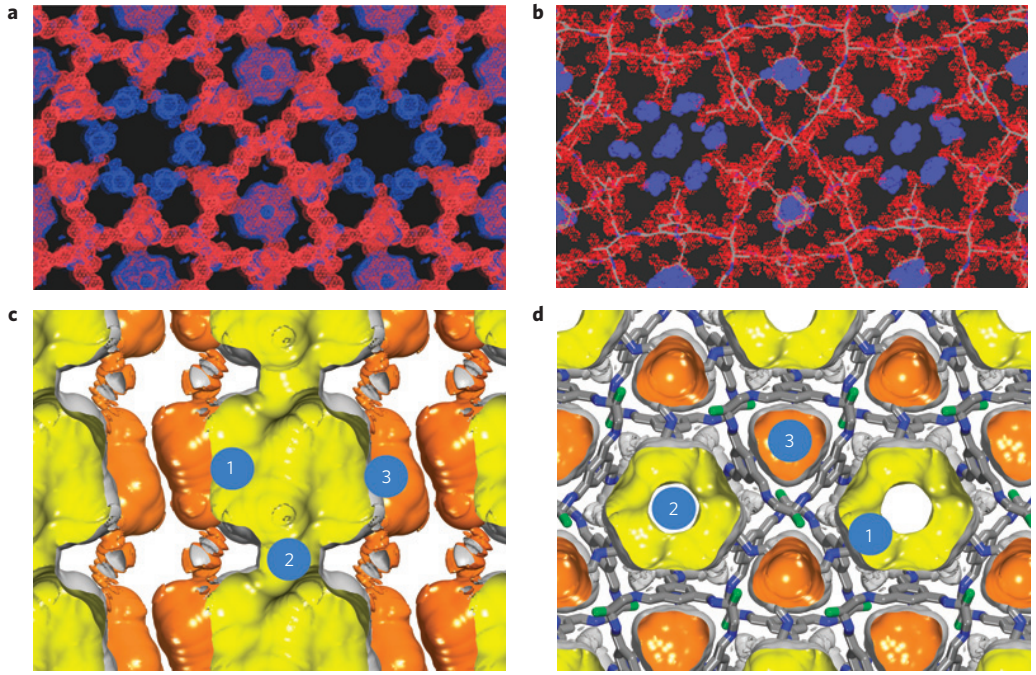

Figure 5 | Molecular simulations suggest that the 0D cage volume contributes to N_2 gas uptake for 2, despite being formally isolated from the 1D pore channels. a, Single-crystal X-ray diffraction data showing an electron density map for the cage **2** framework (in red) and disordered physisorbed water guests (in blue). This map demonstrates that both the 1D channels and the 0D cages are partially occupied by guests before outgassing. **b**, Molecular simulation illustrating the most energetically favourable sites for N_2 adsorption in **2** at saturation (in blue), labelled 1, 2 and 3 in **c**,**d**. **c**,**d**, Schematic showing favoured sorption sites for N_2 as located by molecular simulations for the 2220 isomer of **2**.

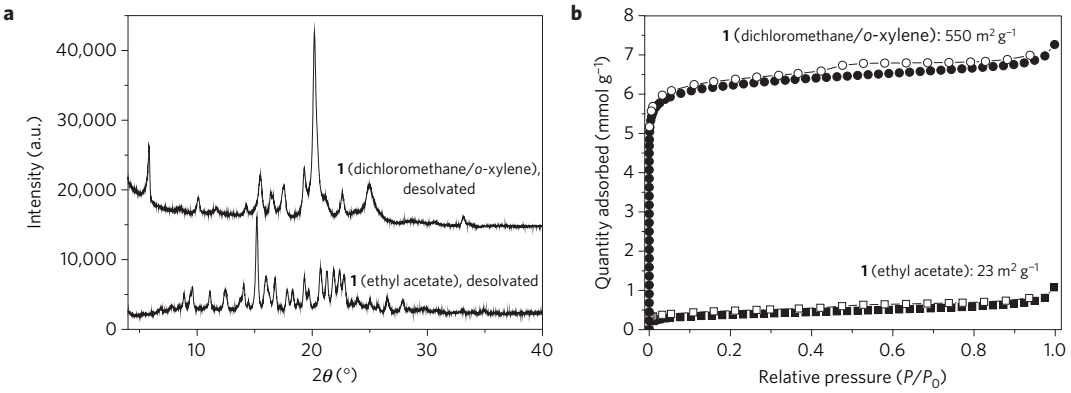

Figure 6 | Recrystallization of 1 forms a permanently porous polymorph. a, Powder X-ray diffraction patterns for desolvated **1** as synthesized in ethyl acetate and recrystallized from a mixture of dichloromethane and *o*-xylene. **b**, N_2 sorption isotherms at 77 K for non-porous and permanently porous polymorphs of **1**, $SA_{BET} = 23\ m^2\ g^{-1}$ and $550\ m^2\ g^{-1}$, respectively. Closed and open symbols denote adsorption and desorption isotherms, respectively. The H_2 uptake at 77 K/1 bar was 1.1 wt%, similar to that observed for **2**.

This points to a wider strategy for the construction of porous materials from cage-like organic building blocks, particularly because the synthesis seems applicable to a number of aliphatic 1,2-diamines. Chirality is inherent to these [4+6] tetrahedral cages and homochiral vertices are readily introduced, for example in **3**. Experiments to investigate further the influence of vertex chirality on crystal packing are underway. The vertex-directed evolution of structure from **1** to **3** suggests that pore volumes might be increased further by incorporating bulkier directing groups at the exo positions. In addition to porous organic crystals, amorphous porous glasses[37] can be foreseen, perhaps by using mixtures of diamines to desymmetrize the cages. Although the three cages reported here decompose before melting, low-melting variants of **1**, **2** or **3** might be conceived to access the first microporous liquids[38]; one potential strategy is suggested by the recent observation of liquid-like behaviour in modified carbon nanotubes[39]. Finally, the two cage-packing modes observed (window-to-arene in **1** and **2**, window-to-window in **3**), coupled with the identification of porous and non-porous polymorphs for **1**, suggests the possibility of materials where porosity can be switched 'on' and 'off', perhaps by means of thermally interconvertible polymorphs. For example, at present, we are searching for systems that trap gas at ambient temperature and pressure by the conversion of a gas-loaded porous cage to its non-porous polymorph.

Methods

Synthesis. A representative synthesis (for cage **1**) is as follows. Ethyl acetate (35 ml) was added to 1,3,5-triformylbenzene (50 mg, 0.31 mmol) in a beaker at room temperature. After 5 min, a solution of ethylene diamine (28 mg, 0.47 mmol) in ethyl acetate (5 ml) was added. The resulting mixture was left covered for 60 h without stirring. A turbid solution was observed to form within 5 min after ethylene diamine

addition to the partially dissolved trialdehyde. This was followed by precipitation of a solid after around 5–6 h and, finally, pale white needles of the solvate $(C_{48}H_{48}N_{12})\cdot 2.5(C_4H_8O_2)$ were observed to crystallize from solution after around 60 h. Compound **1** was obtained by desolvation of the solvate either by heating in air, a flow of dry nitrogen or under reduced pressure. ^{1}HNMR ($CDCl_3$, 400 MHz) δ 8.18 (s, 12H, −CH=N), 7.92 (s, 12H, −ArH), 4.12 (q, $J = 7.2$ Hz, 5H, $2.5\times -OCH_2$), 4.02 (brs, 24H, $-NCH_2$), 2.04 (s, 7.5H, $2.5\times -COCH_3$), 1.25 (t, $J = 7.2$ Hz, 7.5H, $2.5\times CH_3$)ppm. ^{13}CNMR ($CDCl_3$, 100 MHz) δ 171.1, 161.2, 136.4, 129.6, 61.6, 60.4, 21.04, 14.2 ppm. IR (KBr pellet, ν) 2,917 (s), 2,389 (s), 1,739 (s), 1,648 (s), 1,598 (m), 1,433 (m), 1,335 (s), 1,238 (s), 1,155 (s), 1,108 (m) 1,048 (s), 991 (m), 911 (m), 694 (m) cm^{-1}. ESI-MS (CH_3OH) *m/z*: 793 $[M+H]^+$ for $C_{48}H_{48}N_{12}$, 815 $[M+Na]^+$.

Cages **2** and **3** were synthesized by analogous methods using acetonitrile and dichloromethane (or chloroform), respectively, as solvents, see Supplementary Information for details. Unlike **1**, cages **2** and **3** were found to lose their solvent spontaneously at ambient temperature (Supplementary Fig. S19). Both cages **2** and **3**, which are permanently porous, were found to readily adsorb water vapour from the atmosphere unless stored under vacuum or an inert gas.

Characterization. For volumetric gas sorption measurements, samples were degassed offline at 80 °C for 15 h under vacuum (10^{-5} bar) before analysis, followed by degassing on the analysis port under vacuum, also at 80 °C. Isotherms were measured using Micromeritics 2020, 2420 or 2050 instruments, depending on the pressure range required. Gravimetric sorption isotherms were obtained using a HidenIsochema Intelligent Gravimetric Analyser equipped with a micro-gram balance and 2, 100 and 20,000 mbar barotron pressure transducers. Samples were activated by outgassing at 60 °C at 10^{-10} bar until a constant mass had been reached (typically overnight). Data were corrected for buoyancy effects of the system and samples, using the calculated crystallographic densities for the desolvated materials assuming complete desolvation of the structures: cage **1** (1.033 cm^3 g^{-1}), cage **2** (0.874 cm^{3}g^{-1}) and cage **3** (0.973 cm^3 g^{-1}).

Received 6 March 2009; accepted 14 September 2009; published online 25 October 2009

References

1. Barbour, L. J. Crystal porosity and the burden of proof. *Chem. Commun.* 1163–1168 (2006).
2. Cheetham, A. K., Férey, G. & Loiseau, T. Open-framework inorganic materials. *Angew. Chem. Int. Ed.* **38,** 3268–3292 (1999).
3. Kitagawa, S., Kitaura, R. & Noro, S. Functional porous coordination polymers. *Angew. Chem. Int. Ed.* **43,** 2334–2375 (2004).
4. Côté, A. P. *et al.* Porous, crystalline, covalent organic frameworks. *Science* **310,** 1166–1170 (2005).
5. Atwood, J. L., Barbour, L. J. & Jerga, A. Storage of methane and freon by interstitial van der Waals confinement. *Science* **296,** 2367–2368 (2002).
6. Thallapally, P. K. *et al.* Carbon dioxide capture in a self-assembled organic nanochannels. *Chem. Mater.* **19,** 3355–3357 (2007).
7. Thallapally, P. K. *et al.* Gas-induced transformation and expansion of a non-porous organic solid. *Nature Mater.* **7,** 146–150 (2008).
8. Langley, P. J. & Hulliger, J. Nanoporous and mesoporous organic structures: New openings for materials research. *Chem. Soc. Rev.* **28,** 279–291 (1999).
9. Sozzani, P., Bracco, S., Comotti, A., Ferretti, L. & Simonutti, R. Methane and carbon dioxide storage in a porous van der Waals crystal. *Angew. Chem. Int. Ed.* **44,** 1816–1820 (2005).
10. Barrer, R. M. & Shanson, V. H. Dianin's compound as a zeolitic sorbent. *J. Chem. Soc. Chem. Commun.* 333–334 (1976).
11. Lim, S. *et al.* Cucurbit[6]uril: Organic molecular porous material with permanent porosity, exceptional stability, and acetylene sorption properties. *Angew. Chem. Int. Ed.* **47,** 3352–3355 (2008).
12. Comotti, A., Bracco, S., Distefano, G. & Sozzani, P. Methane, carbon dioxide and hydrogen storage in nanoporous dipeptide-based materials. *Chem. Commun.* 284–286 (2009).
13. Sudik, A. C. *et al.* Design, synthesis, structure, and gas (N_2, Ar, CO_2, CH_4, and H_2) sorption properties of porous metal–organic tetrahedral and heterocuboidal polyhedra. *J. Am. Chem. Soc.* **127,** 7110–7118 (2005).
14. Fujita, M. *et al.* Molecular paneling via coordination. *Chem. Commun.* 509–518 (2001).
15. Budd, P. M. *et al.* Polymers of intrinsic microporosity (PIMs): Robust, solution-processable, organic nanoporous materials. *Chem. Commun.* 230–231 (2004).
16. Bradshaw, D. *et al.* Design, chirality, and flexibility in nanoporous molecule-based materials. *Acc. Chem. Res.* **38,** 273–282 (2005).
17. El-Kaderi, H. M. *et al.* Designed synthesis of 3D covalent organic frameworks. *Science* **316,** 268–272 (2007).
18. Kuhn, P., Antonietti, M. & Thomas, A. Porous, covalent triazine-based frameworks prepared by ionothermal synthesis. *Angew. Chem. Int. Ed.* **47,** 3450–3453 (2008).
19. Conway, J. H. & Torquato, S. Packing, tiling, and covering with tetrahedra. *Proc. Natl Acad. Sci. USA* **103,** 10612–10617 (2006).
20. MacGillivray, L. R. & Atwood, J. L. Structural classification and general principles for the design of spherical molecular hosts. *Angew. Chem. Int. Ed.* **38,** 1019–1034 (1999).
21. Furutani, Y. *et al. In situ* spectroscopic, electrochemical, and theoretical studies of the photoinduced host–guest electron transfer that precedes unusual host-mediated alkane photooxidation. *J. Am. Chem. Soc.* **131,** 4764–4768 (2009).
22. Liu, X. J., Liu, Y., Li, G. & Warmuth, R. One-pot, 18-component synthesis of an octahedral nanocontainer molecule. *Angew. Chem. Int. Ed.* **45,** 901–904 (2006).
23. Mastalerz, M. One-pot synthesis of a shape-persistent endo-functionalised nano-sized adamantoid compound. *Chem. Commun.* 4756–4758 (2008).
24. Skowronek, P. & Gawronski, J. Chiral iminospherand of a tetrahedral symmetry spontaneously assembled in a [6+4] cycloaddition. *Org. Lett.* **10,** 4755–4758 (2008).
25. Mecozzi, S. & Rebek, J. The 55% solution: A formula for molecular recognition in the liquid state. *Chem. Eur. J.* **4,** 1016–1022 (1998).
26. Graf, E. & Lehn, J. M. Synthesis and cryptate complexes of a spheroidal macrotricyclic ligand with octahedrotetrahedral coordination. *J. Am. Chem. Soc.* **97,** 5022–5024 (1975).
27. Stang, P. J., Olenyuk, B., Muddiman, D. C. & Smith, R. D. Transition-metal-mediated rational design and self-assembly of chiral, nanoscale supramolecular polyhedra with unique *T* symmetry. *Organometallics* **16,** 3094–3096 (1997).
28. Fiedler, D. *et al.* Selective molecular recognition, C–H bond activation, and catalysis in nanoscale reaction vessels. *Acc. Chem. Res.* **38,** 349–358 (2005).
29. Ajami, D. & Rebek, J. Gas behaviour in self-assembled capsules. *Angew. Chem. Int. Ed.* **47,** 6059–6061 (2008).
30. Iyer, K. S., Norret, M., Dalgarno, S. J., Atwood, J. L. & Raston, C. L. Loading molecular hydrogen cargo within viruslike nanocontainers. *Angew. Chem. Int. Ed.* **47,** 6362–6366 (2008).
31. Soldatov, D. V. *et al.* α- and β-bis(1,1,1-trifluoro-5,5-dimethyl-5-methoxyacetylacetonato)copper(II): Transforming the dense polymorph into a versatile new microporous framework. *J. Am. Chem. Soc.* **121,** 4179–4188 (1999).
32. Soldatov, D. V. & Ripmeester, J. A. Inclusion in microporous β-bis(1,1,1-trifluoro-5,5-dimethyl-5-methoxyacetylacetonato)copper(II), an organic zeolite mimic. *Chem. Mater.* **12,** 1827–1839 (2000).
33. Lin, X. *et al.* High H_2 adsorption by coordination-framework materials. *Angew. Chem. Int. Ed.* **45,** 7358–7364 (2006).
34. Weber, J., Antonietti, M. & Thomas, A. Microporous networks of high-performance polymers: Elastic deformations and gas sorption properties. *Macromolecules* **41,** 2880–2885 (2008).
35. Atwood, J. L., Barbour, L. J., Jerga, A. & Schottel, B. L. Guest transport in a nonporous organic solid via dynamic van der Waals cooperativity. *Science* **298,** 1000–1002 (2002).
36. Banerjee, R. *et al.* Control of pore size and functionality in isoreticular zeolitic imidazolate frameworks and their carbon dioxide selective capture properties. *J. Am. Chem. Soc.* **131,** 3875–3877 (2009).
37. Tian, J., Thallapally, P. K., Dalgarno, S. J., McGrail, P. B. & Atwood, J. L. Amorphous molecular organic solids for gas adsorption. *Angew. Chem. Int. Ed.* **48,** 5492–5495 (2009).
38. O'Reilly, N., Giri, N. & James, S. L. Porous liquids. *Chem. Eur. J.* **13,** 3020–3025 (2007).
39. Zhang, J.-X., Zheng, Y.-P., Yu, P.-Y., Mo, S. & Wang, R.-M. Modified carbon nanotubes with liquid-like behaviour at 45 °C. *Carbon* **47,** 2776–2781 (2009).

Acknowledgements

We thank the Engineering and Physical Sciences Research Council (EPSRC) for financial support under grant EPSRC/C511794 and Kaneka Corporation, Japan, for financial supporting a research visit for T.T. We thank the STFC for access to Diamond and M.J. Rosseinsky for helpful advice. A.C. is a Royal Society Wolfson Research Merit Award holder.

Author contributions

T.T., S.I.S., S.J., D.J.A. and S.S. synthesized cages **1–3**, J.T.A.J. and R.C. carried out volumetric sorption measurements, D.B. carried out gravimetric sorption measurements, T.H. carried out microscopy, desolvation studies and TGA, A.T. constructed the molecular models and carried out the sorption simulations, J.B., A.M.Z.S., S.Y.C., C.T., S.T., J.P. and A.S. carried out the crystallography; in particular J.B. and A.S. solved the crucial first structure for the cage **1** ethyl acetate solvate. J.T.A.J. discovered the porous polymorph of **1**. A.I.C. conceived the experiments; all authors contributed to writing the paper.

Additional information

Supplementary information accompanies this paper on www.nature.com/naturematerials. Reprints and permissions information is available online at http://npg.nature.com/reprintsandpermissions. Correspondence and requests for materials should be addressed to A.I.C.